JITH 2017
18èmes Journées Internationales de Thermique (JITH 2017)
Monastir (Tunisie), 25 - 27 Octobre 2017

A three-dimensional inverse source problem in radiative transfer

Hajer GRISSA, Faouzi ASKRI, Sassi BEN NASRALLAH
Ecole Nationale d'Ingénieurs de Monastir, Laboratoire d'Etudes des Systèmes Thermiques et Energétiques
Monastir, Tunisia
grissahajer@yahoo.fr

Abstract: The control volume finite element method (CVFEM) is employed to solve an inverse radition problem of source term in three-dimensional medium. The inverse problem is formulated as an optimization problem between the calculated and the experimental data and is solved by the Levenberg Marquardt method (LMM). The effects of measurement error, radiative parameters and number of measurement points on the accuracy of the inverse problem are investigated. The CVFEM-LMM combination, which is applied, to the knowledge of the author, for the first time to solve inverse source problem in 3-D enclosure, has been found to accurately predict the temperature distribution.

Keywords :

Inverse radiation, source problem, CVFEM.

1. Introduction

Inverse radiation problems governed by the integro-differential equation of radiative transfer have been studied extensively for their practical applications. The inverse analysis can be applied to determine the radiative properties of a medium or the boundary conditions or the source problem.
Only a limited number of works is available in the literature on the solution of the inverse source radiation problems involving 3-D geometry. In fact, most of the work has considered one-dimensional [1-5] or two-dimensional [6-10] system.
For three-dimensional problems, Wang et al. [11], have presented an inverse radiation analysis based on the backward Monte Carlo method in a large rectangular enclosure using radiative intensities in the visible range. Liu et al. [12] have solved the temperature field in an inhomogeneous, absorbing, emitting and anisotropically scattering media from the knowledge of the exit radiative energy received by charge- coupled device cameras.

The main objective of this paper is to examine the accuracy of the CVFEM for estimating the 3-D temperature distribution in an absorbing, emitting and anisotropically scattering media. The analysis consists of the direct problem and the inverse problem. The effects of various variables such as errors in the measured data, number of sensors and system parameters on the accuracy of the inverse analysis will be investigated.

2. Analysis

2.1 Direct problem

We consider an absorbing, emitting, scattering and gray medium. In this case, the mathematical formulation of the direct problem is given by

$$\nabla.\left(I(s,\boldsymbol{\Omega})\boldsymbol{\Omega}\right) = -(k_a + k_d)I(s,\boldsymbol{\Omega}) + S(s) + \frac{k_d}{4\Pi}\int_{4\Pi} I(s,\boldsymbol{\Omega}')P(\boldsymbol{\Omega},\boldsymbol{\Omega}')d\,\Omega' \qquad (1)$$

where $I(s,\boldsymbol{\Omega})$ is the radiative intensity at position s in the direction $\boldsymbol{\Omega}$, k_a and k_d are absorption and scattering coefficients, respectively, $P(\boldsymbol{\Omega},\boldsymbol{\Omega}')$ is the scattering phase function from the incoming direction $\boldsymbol{\Omega}'$ to the outgoing direction $\boldsymbol{\Omega}$ and $S(s)$ is the source term related to the temperature in the medium $T(s)$ by

$$S(s) = \frac{\sigma_{sb}k_a T(s)^4}{\pi} \qquad (2)$$

The medium boundary surface is assumed gray and emits and reflects diffusely. So, the radiation boundary condition can be written as

$$I_w(\boldsymbol{\Omega}) = \frac{\varepsilon_w \sigma_{sb} T_w^4}{\pi} + \frac{1-\varepsilon_w}{\pi} \int_{\boldsymbol{\Omega}'.\boldsymbol{n_w}<0} I_w(\boldsymbol{\Omega}')|\boldsymbol{\Omega}'.\boldsymbol{n_w}|d\Omega' \qquad if \quad \boldsymbol{\Omega}.\boldsymbol{n_w} > 0 \tag{3}$$

where ε_w is the wall emissivity, σ_{sb} is the Stefan-Boltzman constant and $\boldsymbol{n_w}$ is the unit normal vector to the wall.

In the CVFEM, the spatial and the angular domains are divided into a finite number of control volumes and control solid angles, respectively.

For the angular domain discretization (Figure 1), the total solid angle (i.e. 4π) is subdivided into $(N_\theta \times N_\varphi)$ control solid angles $\Delta\Omega^{mn}$ as

$$\Delta\Omega^{mn} = \int_{\varphi^-}^{\varphi^+} \int_{\theta^-}^{\theta^+} sin\theta d\theta d\varphi \tag{4}$$

where

N_θ : the number of control angles in the polar angle θ

N_φ: the number of control angles in the azimuthal angle φ

$\Delta\theta$: the elementary polar angle as follows Δ

$$\Delta\theta = \theta^+ - \theta^- = \frac{\pi}{N_\theta} \tag{5}$$

$$\begin{cases} \theta^- = (m-1)\Delta\theta \\ \theta^+ = m\Delta\theta \end{cases}, \quad m = 1,..,N_\theta \tag{6}$$

$\Delta\varphi$: the elementary azimuthal angle as follows

$$\Delta\varphi = \varphi^+ - \varphi^- = \frac{2\pi}{N_\varphi} \tag{7}$$

$$\begin{cases} \varphi^- = (n-1)\Delta\varphi \\ \varphi^+ = n\Delta\varphi \end{cases}, \quad n = 1,..,N_\varphi \tag{8}$$

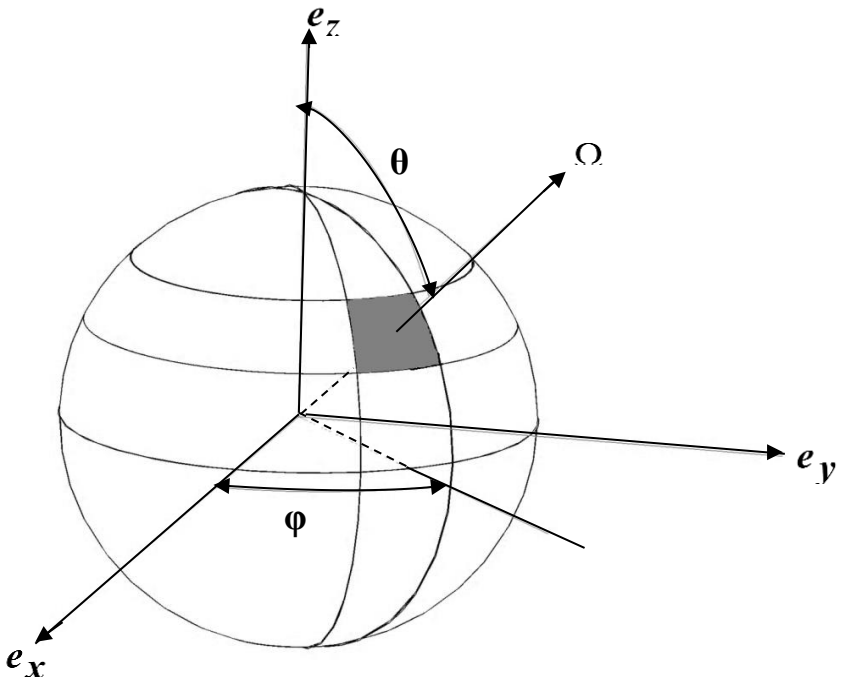

Figure 1 Angular discretization

For spatial discretization, the domain $(\boldsymbol{e_x}, \boldsymbol{e_y})$ is subdivided into three-node triangular elements and control surfaces are created around each node *N* by joining the controids of the elements to midpoints of the corresponding sides (Fig. 2a). Then, to create the control volume ΔV_{ijk} (Fig. 2b), the control surface is multiplied by Δz for nodes within calculation domain (and by Δz/2 when nodes are in boundaries) where Δz is the step of calculation in $\boldsymbol{e_z}$ direction.

After angular and spatial discretization, the radiative transfer equation is integrated over both control volume and control solid angle

$$\int_{\Delta V_{ijk}} \int_{\Delta\Omega^{mn}} \nabla.(I(s,\boldsymbol{\Omega})\boldsymbol{\Omega}) d\Omega dV = -\int_{\Delta V_{ijk}} \int_{\Delta\Omega^{mn}} (k_a + k_d) I(s,\boldsymbol{\Omega}) d\Omega dV \quad (9)$$
$$+ \int_{\Delta V_{ijk}} \int_{\Delta\Omega^{mn}} S(s) d\Omega dV + \int_{\Delta V_{ijk}} \int_{\Delta\Omega^{mn}} \frac{k_d}{4\Pi} \int_{4\Pi} I(s,\boldsymbol{\Omega}') P(\boldsymbol{\Omega},\boldsymbol{\Omega}') d\,\Omega' d\Omega dV$$

To approximate the integrals that represent the extinction; emission and in-scattering contributions, the radiation intensity is considered constant within ΔV_{ijk} and $\Delta\Omega^{mn}$ and is evaluated at the centroid of the control volume and at the centre direction of the control solid angle. Then, the obtained algebraic equation of the RTE is formulated as a matrix system and is solved using the conditioned conjugate gradient squared method (CCGS). A detailed calculation can be found in Ref. [13].

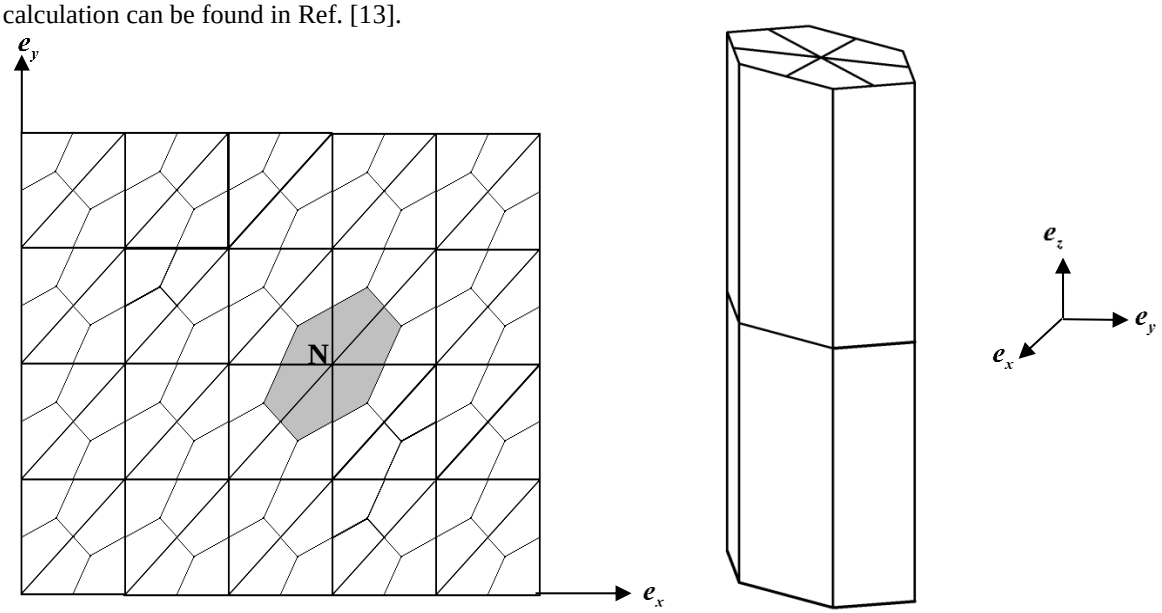

(a) **(b)**

Figure 2 Spatial discretization. (a): Discretization in $(\boldsymbol{e_x}, \boldsymbol{e_y})$ plane, (b): Control volume ΔV_{ijk}.

2.1. Inverse radiation problem

The estimation of the temperature distribution is achieved by a minimization of the objective function defined in Eq.(10). This function is expressed by the summation of the squared residues between computed incident radiation heat fluxes obtained from direct problem, $q_i(\beta)$, and measured incident radiation heat fluxes, Y_i, at i measurement position

$$J(\boldsymbol{\beta}) = \sum_{i=1}^{l} \left(Y_i - q_i(\boldsymbol{\beta})\right)^2 \quad (10)$$

where l is the total number of the measurement points and $\boldsymbol{\beta}$ is the vector of unknowns.

The minimization of the objective function is performed by the Levenberg Marquardt method.
The Eq.(10) can be written as follows

$$J = \boldsymbol{D}^T \boldsymbol{D} \quad (11)$$

where D_i is the difference between the measured and computed incident radiation heat fluxes

$$D_i = Y_i - q_i(\boldsymbol{\beta}) \quad (12)$$

Minimizing *J* with respect to $\boldsymbol{\beta}$ is equivalent to make its derivates equal to zero

$$\frac{\partial J}{\partial \beta} = \frac{\partial (\boldsymbol{D}^T \boldsymbol{D})}{\partial \boldsymbol{\beta}} = 0 \tag{13}$$

In this equation, the vector $\boldsymbol{D}$ is expanded in a Taylor series and only the first order terms are retained. To damp oscillations and instabilities due to the ill-conditioned character of the problem, a damping parameter, λ, is added to yield the LMM. The iterative process is expressed as

$$\boldsymbol{\beta}^{k+1} = \boldsymbol{\beta}^k + \Delta\boldsymbol{\beta}^k \tag{14}$$

where

$$\Delta\boldsymbol{\beta}^k = [(\boldsymbol{X}^k)^T \boldsymbol{X}^k + \lambda^k \boldsymbol{I}]^{-1} (\boldsymbol{X}^k)^T \boldsymbol{D}^k \tag{15}$$

$\boldsymbol{I}$ and $\boldsymbol{X}$ denote the identity and the sensitivity matrix, respectively and the superscript k denotes the iteration number.

The elements of sensitivity matrix, X_{ij} , are defined as the first derivative of the incident radiation heat flux at i measurement position, $\partial q_i(\boldsymbol{\beta})$, with respect to the unknown parameter,β_j , that is,

$$X_{ij} = \frac{\partial q_i(\boldsymbol{\beta})}{\partial \beta_j}, \qquad i = 1, \dots, l \ \ and \ j = 1, \dots, n_p \tag{16}$$

The iterative procedure is continued until the convergence criterion

$$|\boldsymbol{\beta}^{k+1} - \boldsymbol{\beta}^k| < 10^{-5} \tag{17}$$

is satisfied.

3. Results

In order to obtain the measurement incident radiative heat flux at boundary surfaces, the direct problem is solved with known source term. Then, the obtained numerical solutions are considered as experimental data after adding small random noise:

$$\boldsymbol{Y} = \boldsymbol{q}_{w,exact} + \zeta\sigma \tag{18}$$

where ζ is the Gaussian distributed random error within -2.576 to 2.576 for a 99% confidence bounds and σ is the standard deviation of measured radiative heat flux.

We consider a three dimensional furnace (1m×1m×1m) enclosing an absorbing, emitting and anisotropic scattering medium. The scattering phase function of medium is assumed to be linear anisotropic, given as

$$P(\boldsymbol{\Omega}, \boldsymbol{\Omega}') = 1 + g\boldsymbol{\Omega}.\boldsymbol{\Omega}' \tag{19}$$

where g is the scattering asymmetry parameter.

The temperature distribution in the medium is considered as follows

$$T(\boldsymbol{s}) = 100 + 35x + 20y + 15z \tag{20}$$

Table 1 shows the specified values of the known parameters.

k_a (m^{-1})	k_d (m^{-1})	g	ε_w
0.5	0.5	1.0	0.5

Table 1: Specified values of the known parameters.

The CVFEM is used to predict the incident radiative heat flux with $(N_x \times N_y \times N_z)$ spatial control volumes and (6×4) control solid angles.

For the sake of comparison, the maximum relative error E_{max}, the root mean square error E_{rms} and the average temperature T_{av} are defined as following

$$E_{max} = 100 \times max \left| \frac{T_{estimated}(s) - T_{exact}(s)}{T_{exact}(s)} \right|, \qquad \% \tag{21}$$

$$E_{rms} = \left\{ \frac{1}{L_x L_y L_z} \int_0^{L_x} \int_0^{L_y} \int_0^{L_z} [T_{estimated}(s) - T_{exact}(s)]^2 dx dy dz \right\}^{1/2} \tag{22}$$

$$T_{av} = \frac{1}{L_x L_y L_z} \int_0^{L_x} \int_0^{L_y} \int_0^{L_z} T(s) dx dy dz \tag{23}$$

Case1

Table 2 shows the maximum relative errors of the temperature estimation for three different measurement error values of incident radiative heat fluxes on the walls. Two numbers of sensors used to measure incident radiative heat flux are considered $l = 36$ and $l = 12$ which corresponds to $N_x = N_y = N_z = 15$ and $N_x = N_y = N_z = 7$, respectively.

From table 2 we note that increasing the standard deviation σ from 0 to 0.1, the accuracy of the estimation decreases and increasing the number of sensors I from 12 to 36, the accuracy of the estimation is improved obviously. When there is no measurement error in the data, the reduction of number of measurement points doesn't affect the accuracy of estimation.

σ	0		0.005		0.1	
I	36	12	36	12	36	12
E_{max} (٪)	1. 29 10^{-3}	1. 29 10^{-3}	0.14	0.30	1.92	3.97
E_{rms} (K)	1.08 10^{-3}	1.08 10^{-3}	7.58 10^{-2}	0.12	1.07	2.25
E_{rms}/T_{av} (٪)	8.00 10^{-4}	8.00 10^{-4}	5.62 10^{-2}	9.5 10^{-2}	0.797	1.66

Table 2: Maximum relative errors and RMS errors of the temperature estimation for different measurement error and for I = 36 and 12.

Case2

The effects of radiative parameter and boundary conditions on the accuracy of the inverse estimation are studied. It is assumed that the measured incident radiative heat fluxes have no measurement error. All the parameters are constant and equal the values mentioned in Table 1, except for the parameter that its effects are studied. The number of sensors is set equal to 12.

The effects of absorption coefficient on the accuracy of inverse solution are shown in Figure 3. This figure shows the RMS error, E_{rms}, versus absorption coefficient. As shown in Figure 3, within the range from $k_a = 0$, to 1 m^{-1}, all of the RMS errors are less than 0.09 K. The effects of absorption coefficient on the estimation are very small.

The effects of wall emissivity on the inverse solution are shown in Figure 4. As shown in Figure 4, within the range from 0 to 1, the curve has a minimum in $\varepsilon_w = 0.5$ and the maximum RMS error is less than 0.7 K. The effects of wall emissivity are considered as small.

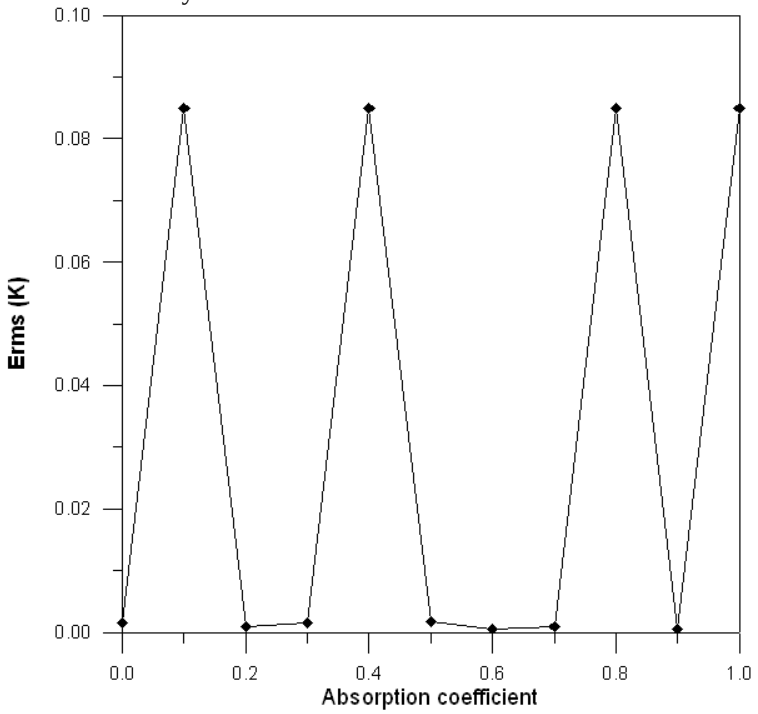

Figure 3 Effects of absorption coefficient on the temperature estimation.

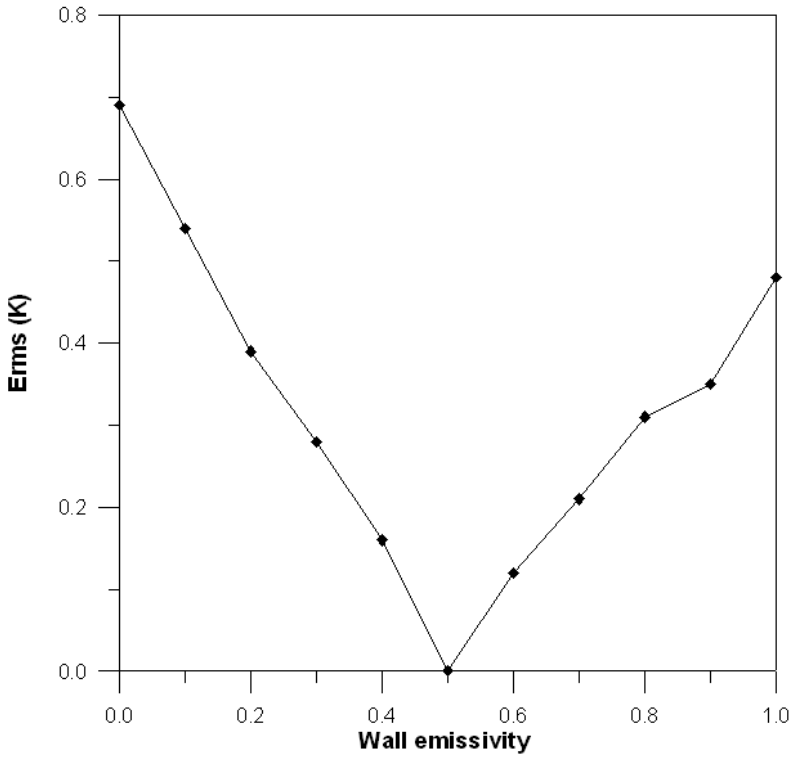

Figure 4 Effects of wall emissivity on the temperature estimation.

Case 3

In the practical processes of measurement and inverse solution, the parameters given in Table 1 may have more or less random errors. In order to examine the effects of these errors on temperature estimation, it is assumed that all these parameters have normally distributed random errors and are produced as follows

$$\odot_j = \odot_j\big|_{exact} + \sigma_{\odot_j}\zeta \qquad (24)$$

Here $\odot_j$ could be absorption coefficient, scattering coefficient, wall emissivity or scattering asymmetry parameter. $\odot_j\big|_{exact}$ is the exact related value, which is brought in Table 1. $\sigma_{\odot_j}$ is the standard deviation of the parameter $\odot_j$. Table 3 shows the maximum relative errors and the RMS errors of the temperature estimation for two different measurement error values of parameters with exact incident radiation heat fluxes ($\sigma = 0.0$). The number of sensors is set equal to 12. It can be seen that the combined effects of the random errors of absorption coefficient, scattering coefficient, wall emissivity and scattering asymmetry parameter on the temperature estimation are small.

$\sigma_{\odot_j}$	**0.005**	**0.1**
$\mathbf{E_{max}}$ (٪)	0.13	0.85
$\mathbf{E_{rms}}$ **(K)**	8.17 10^{-2}	0.35
$\mathbf{E_{rms}/T_{av}}$ (٪)	6.05 10^{-2}	0.26

Table 3: Maximum relative errors and RMS errors of the of the temperature estimation for errors in system parameters with exact incident radiation heat fluxes for l = 12.

In a real problem, existing errors in both measured data and system radiative parameters are probable. To study the combined effects of these errors on the temperature estimation, we consider in Table 4 different cases of the combination of σ and $\sigma_{\odot_j}$. Comparing Table 4 with Table 3 shows that the temperature estimation is more sensitive to existing errors in measurement errors of the incident radiative heat fluxes than errors in system parameters. As shown in Table 4, the reconstruction of the temperature is good even with noisy input data.

$\sigma = \sigma_{\odot_j}$	**0.005**	**0.1**
$\mathbf{E_{max}}$ (٪)	0.29	4.23
$\mathbf{E_{rms}}$ **(K)**	0.13	2.31
$\mathbf{E_{rms}/T_{av}}$ (٪)	9.8 10^{-2}	1.71

Table 4: Maximum relative errors and RMS errors of the temperature estimation for errors in system parameters and measured data for l = 12.

4. Conclusion

An inverse radiation problem is solved for the temperature estimation in an absorbing, emitting and anisotropically scattering medium confined in a three dimensional furnace from the knowledge of incident radiative heat fluxes on the boundaries. The radiative transfer equation is solved by the CVFEM and the optimization is achieved using the LMM. Three test cases involving different number of sensors, system parameters and measurement errors are considered. The results of this study show that the CVFEM-LMM combination can predict accurately the 3-D temperature distribution.

References

[1] L.H. Liu, H.P. Tan, Q.Z. Yu, Simultaneous identification of temperature profile and wall emissivities in semitransparent medium by inverse radiation analysis, Numer. Heat Tran., Part A 36 (1999), 511–525.

[2] L.H. Liu, H.P. Tan, Q.Z. Yu, Inverse radiation problem in one-dimensional semitransparent plane-parallel media with opaque and specularly reflecting boundaries, J. Quant. Spectrosc. Radiative Transfer, 64 (2000), 395–407.

[3] H.C. Zhou, Y.B. Hou, D.L. Chen, C.G. Zheng, An inverse radiative transfer problem of simultaneously estimating profiles of temperature and radiative parameters from boundary intensity and temperature measurements, J. Quant. Spectrosc. Radiative Transfer, 74 (2002), 605-620,

[4] A. Namjoo, S.M. Hosseini Sarvari , A. Behzadmehr, S.H. Mansouri , Inverse radiation problem of temperature distribution in one-dimensional isotropically scattering participating slab with variable refractive index, J. Quant. Spectrosc. Radiative Transfer, 110 (2009), 491-505,

[5] H. Qi , D.L. Wang, S.G. Wang, L.M. Ruan, Inverse transient radiation analysis in one-dimensional non-homogeneous participating slabs using particle swarm optimization algorithms, J. Quant. Spectrosc. Radiative Transfer, 112 (2011), 2507-2519

[6] L.H. Liu, J. Jiang, Inverse radiation problem for reconstruction of temperature profile in axisymmetric free flames, J. Quant. Spectrosc. Radiative Transfer, 70 (2001), 207–215.

[7] H. Fan, B. Li, L. Yang, R. Wang, Solution of the inverse radiative load problem in a two-dimensional system, J. Quant. Spectrosc. Radiative Transfer , 74 (2002), 85-95.

[8] D. Liu, J.H. Yan, F. Wang, Q.X. Huang, Y. Chi, K.F. Cen, Inverse radiation analysis of simultaneous estimation of temperature field and radiative properties in a two-dimensional participating medium, Int. J. Heat Mass Transfer, (2010), 4474-4481.

[9] T. Salinas Carlos, Inverse radiation analysis in two-dimensional gray media using the discrete ordinates method with a multidimensional scheme, International Journal of Thermal Sciences, 49 (2010), 302-310.

[10] D. Liu, J.H. Yan, F. Wang, Q.X. Huang, Y. Chi, K.F. Cen, Experimental reconstructions of flame temperature distributions in laboratory-scale and large-scale pulverized-coal fired furnaces by inverse radiation analysis, Fuel, 39 (2012), 397-403.

[11] L.H. Liu, H.P. Tan, Z.H. He, Inverse radiation problem of source term in three-dimensional complicated geometric semitransparent media, International Journal of Thermal sciences, 40 (2001), 528–538

[12] F. Wang , D. Liu , K.F. Cen, J.H. Yan, Q.X. Huang, Y. Chi , Efficient inverse radiation analysis of temperature distribution in participating medium based on backward Monte Carlo method, J. Quant. Spectrosc. Radiative Transfer, 109 (2008), 2171-2181.

[13] H. Grissa, , F. Askri, , M. Ben Salah, S. Ben Nasrallah, Three-dimensional radiative transfer modeling using the control volume finite element method, J. Quantitative Spectroscopy Radiative Transfer, 105 (2007), 388-404.